NANO LETTERS

pubs.acs.org/NanoLett Letter

Crystalline Silicon White Light Sources Driven by Optical Resonances

Jin Xiang, Mincheng Panmai, Shuwen Bai, Yuhao Ren, Guang-Can Li, Shulei Li, Jin Liu, Juntao Li,* Miaoxuan Zeng, Juncong She, Yi Xu, and Sheng Lan*

Cite This: https://dx.doi.org/10.1021/acs.nanolett.0c04314 Read Online

ACCESS | Metrics & More | Article Recommendations | Supporting Information

ABSTRACT: Silicon (Si) is generally considered as a poor photon emitter, and various scenarios have been proposed to improve the photon emission efficiency of Si. Here, we report the observation of a burst of the hot electron luminescence from Si nanoparticles with diameters of 150−250 nm, which is triggered by the exponential increase of the carrier density at high temperatures. We show that the stable white light emission above the threshold can be realized by resonantly exciting either the mirror-image-induced magnetic dipole resonance of a Si nanoparticle placed on a thin silver film or the surface lattice resonance of a regular array of Si nanopillars with femtosecond laser pulses of only a few picojoules, where significant enhancements in two- and three-photon-induced absorption can be achieved. Our findings indicate the possibility of realizing all-Si-based nanolasers with manipulated emission wavelength, which can be easily incorporated into future integrated optical circuits.

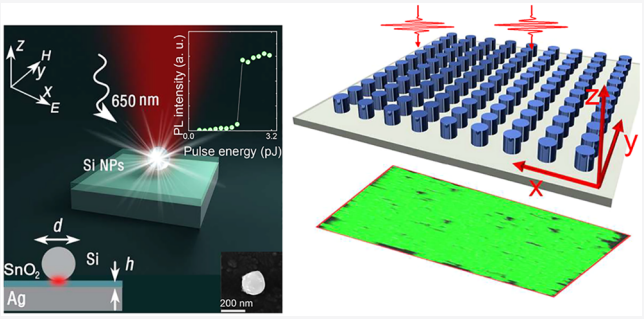

KEYWORDS: *Si nanoparticle, Mie resonance, thin metal film, surface lattice resonance, hot electron luminescence, femtosecond laser pulse*

INTRODUCTION

Silicon (Si) has demonstrated its superior properties in making electronic devices, optical waveguides and detectors, solar cells, and so on.[1] All-Si-based integrated circuits for all-optical signal processing have been the dream of scientists and engineers.[2,3] Basically, light emitters, waveguides, and detectors are considered as the key components for optical computation which requires signal generation, transportation, and detection. So far, Si has been proven as a good material for making waveguides and detectors.[4,5] However, crystalline Si light sources compatible with the current fabrication technology still remain as a big challenge although those made of Si quantum dots or porous Si have been demonstrated.[6−9] Hence, the effort devoted to Si-based light emitters never stops, and direct bandgap emission from hexagonal Ge and Si/Ge alloys has been realized.[10] Recently, Si nanoparticles with diameters ranging from 150−250 nm have attracted great interest owing to the existence of Mie resonances which can be exploited to manipulate their scattering properties.[10−15] Directional scattering of a Si nanoparticle has been demonstrated by exploiting the interference of its electric dipole (ED) and magnetic dipole (MD).[16−18] More interestingly, the significantly enhanced electric field achieved at the Mie resonances can be employed to enhance the nonlinear optical responses of high-index dielectric nanoparticles, such as harmonic generation, hot electron luminescence, and even lasing.[19−27]

RESULTS AND DISCUSSION

Recently, luminescence originating from the relaxation of hot electrons within the conduction band, which is quite similar to that observed in single plasmonic hot spots,[28] was observed in GaAs nanoparticles.[29] In contrast, luminescence resulting from the interband transition of hot electrons was found in Si nanowires coated with silver (Ag) films.[30] Similarly, luminescence arising from the vertical transition of hot electrons was realized in Si quantum dots by utilizing the Auger effect.[6] Very recently, it was demonstrated that interband transition of hot electrons can also be realized in Si nanoparticles by exploiting the MD-enhanced two- and three-photon-induced absorption (2PA and 3PA) and the magnetic quadrupole (MQ)/electric quadrupole (EQ)-enhanced radiative recombination.[23,24] This strategy is illustrated in Figure 1a where the Auger effect plays a crucial role in significantly enhancing the quantum efficiency. However, it is apparent that a large carrier density at the Δ valley is necessary in order to fully exploit this effect. Fortunately, this

Received: November 3, 2020
Revised: March 8, 2021

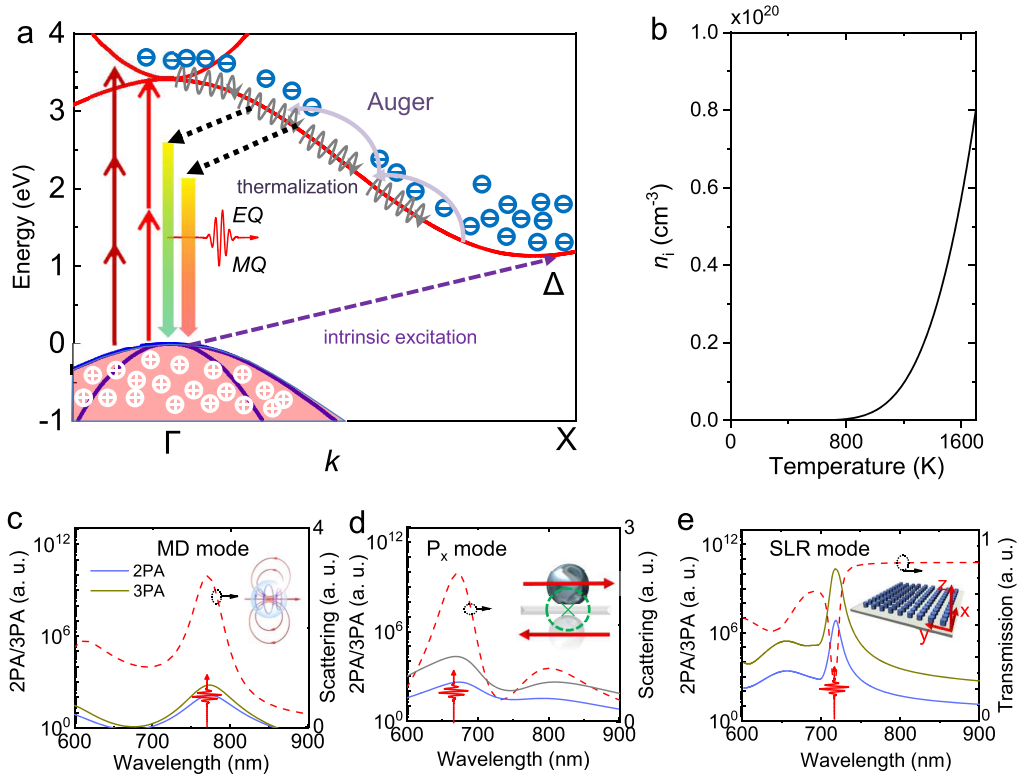

Figure 1. Quantum efficiency enhanced by resonantly exciting the optical resonances of various structures composed of Si nanoparticles. (a) Energy band diagram of Si in which the optical processes and carrier dynamics responsible for the generation and recombination of hot electrons are illustrated. Δ is the minimum of the conduction band. (b) Dependence of intrinsic carrier density on temperature calculated for Si. (c) MD resonance excited in a Si nanoparticle (dashed curve) suspended in air and the enhanced 2PA and 3PA at the resonance (solid curves). (d) Mirror-image-induced MD resonance excited in a Si nanoparticle located on a thin Ag film (dashed curve) and the enhanced 2PA and 3PA at the resonance (solid curves). (e) Surface lattice resonance excited in a regular array of Si nanopillars (dashed curve) and the enhanced 2PA and 3PA at the resonance (solid curves). In each case of (c), (d), and (e), the structure used to generate the optical resonance is shown in the inset.

requirement can be fulfilled by utilizing the heat released by the thermalization of hot electrons, which may trigger the intrinsic excitation in the Si nanoparticle and lead to an exponential increase of carrier density, as shown in Figure 1b. Actually, the high temperature necessary for triggering the intrinsic excitation of carriers can be achieved by injecting dense electron−hole plasma via the optical resonances of the Si nanoparticle (Note 1, Supporting Information).

Basically, the quantum efficiency of the luminescence can be expressed as follows:

$$\eta = \frac{1}{1 + \frac{\tau_r}{\tau_{nr}}} \tag{1}$$

where τ_r and τ_{nr} denote the radiative and nonradiative recombination lifetimes of carriers. So far, much effort has been devoted to the reduction of τ_r and less attention has been paid to the increase of τ_{nr}. Our previous work demonstrates that the quantum efficiency of the interband transition in Si nanoparticles can also be significantly enhanced by increasing τ_{nr} through the Auger effect.[23] We also indicated that carrier dynamics could be modified dramatically by injecting dense electron−hole plasma.[24]

Physically, τ_r is no longer a constant in the case of high injection, and it becomes inversely proportional to the injected carrier density Δn,[31] i.e.,

$$\tau_{rh} = \frac{1}{B_r \Delta n} \tag{2}$$

Here, τ_{rh} is the radiative recombination lifetime at high injection and B_r is the rate of radiative capture probability. On the other hand, τ_{nr} can be prolonged by exploiting the Auger process whose lifetime (τ_{Au}) is inversely proportional to the square of Δn,[31] i.e.,

$$\tau_{Auh} \propto \frac{\tau_{Au}}{(\Delta n)^2} \tag{3}$$

Based on the above equations, it is found that the quantum efficiency can be enhanced by orders of magnitude through injecting high-density carriers (Figure S1, Supporting Information).

Now we compare the carrier densities generated in three types of spherical Si particles with diameters (d) that differ by one order of magnitude, including a quantum dot with $d \sim 18$ nm, a nanoparticle with $d \sim 180$ nm, and a microparticle with $d \sim 1.8$ μm. It is found that the largest carrier density is achieved in the Si nanoparticle which possesses Mie resonances with line widths comparable to that of the femtosecond laser pulses. If the carrier generation is dominated by 2PA, then the carrier density generated in the Si nanoparticle is four orders of magnitude larger than that in the Si quantum dot and about 50 times larger than that in the Si microparticle (Figure S2, Supporting Information). Based on our previous studies, the nonlinear optical responses of Si nanoparticles smaller than 100 nm are quite weak owing to the lack of optical resonances in the visible-to-near-infrared spectral range.

https://dx.doi.org/10.1021/acs.nanolett.0c04314
Nano Lett. XXXX, XXX, XXX−XXX

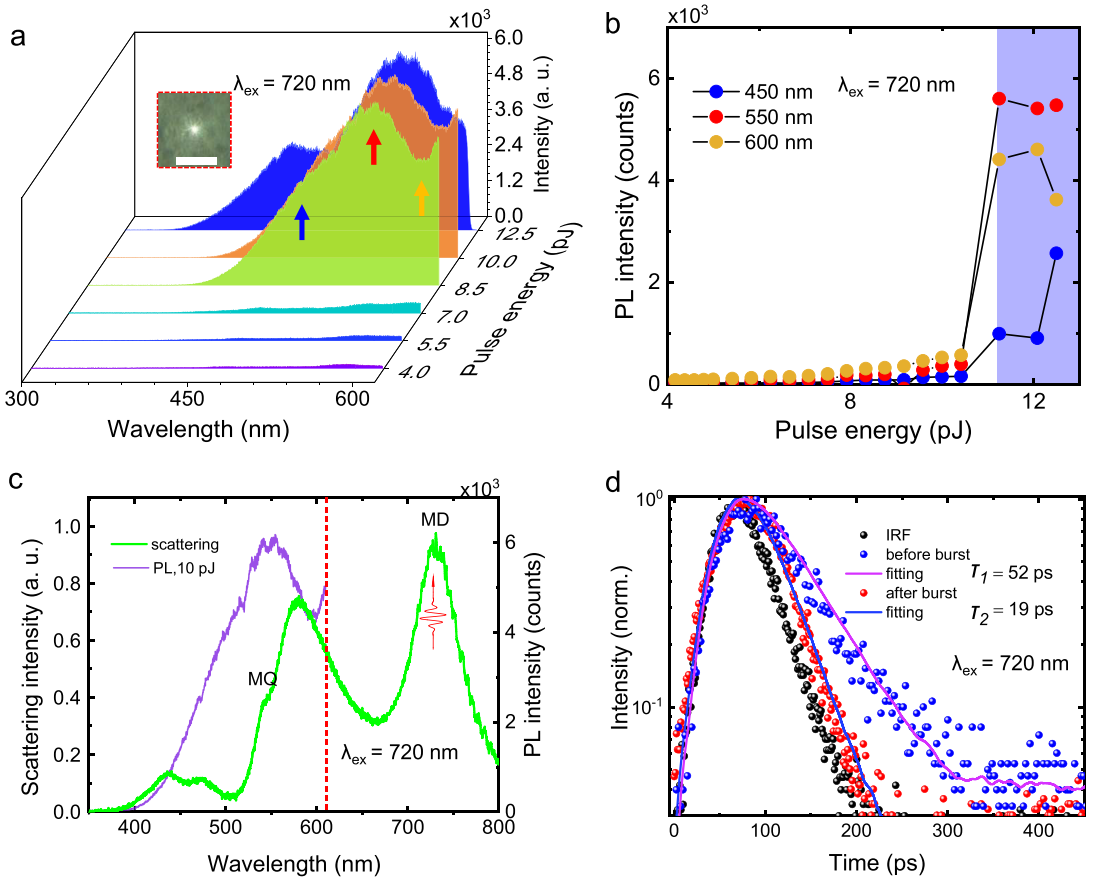

Figure 2. Luminescence burst observed for Si nanoparticles on a SiO_2 substrate. (a) Evolution of the luminescence spectrum of a Si nanoparticle (on a SiO_2 substrate) with increasing excitation pulse energy observed by resonantly exciting the MD resonance of the Si nanoparticle. The diameter of the Si nanoparticle is $d \sim 180$ nm. The image of the luminescent Si nanoparticle above the threshold recorded by using a charge coupled device is shown in the inset. The length of the scale bar is 10 μm. (b) Dependence of the luminescence intensity on the excitation pulse energy observed at three different wavelengths marked by colored arrows in (a). (c) Comparison of the luminescence spectrum of the Si nanoparticle above the threshold with its scattering spectrum. The dotted line indicates the cutoff wavelength of the short-pass filter used in the measurements. (d) Luminescence decays measured for the Si nanoparticle at excitation pulse energies below and above the threshold (for the burst of the luminescence). Also shown is the instrument response function (IRF) which gives the time resolution of the luminescence lifetime. The excitation wavelength was chosen to be λ_{ex}= 720 nm.

In Figure 1c–e, we show schematically various optical resonances which can be utilized to enhance the 2PA and 3PA of Si nanoparticles. Apart from the Mie resonances supported by a Si nanoparticle on a silica (SiO_2) substrate (Figure 1c), the mirror-image-induced MD resonance formed in a Si nanoparticle placed on a metal film (Figure 1d) and the surface lattice resonance (SLR) formed in a regular array of Si nanopillars (Figure 1e) can also be exploited to enhance the nonlinear optical responses of Si nanoparticles.

From Figure 1a, it is noticed that the lift of electrons from the valence band to the conduction band of Si can be realized through a 2PA or 3PA process. For laser wavelengths smaller than 720 nm, the carrier generation would be dominated by a 2PA process, which is more efficient. Here, we chose a Si nanoparticle on the SiO_2 substrate and excited its MD resonance at ~720 nm. The luminescence spectrum in the short-wavelength side was measured as a function of the pulse energy, as shown in Figure 2a. For pulse energies lower than 8.5 pJ, the luminescence intensity increases gradually with increasing pulse energy. However, a dramatic increase in the luminescence intensity by one order of magnitude was observed when the pulse energy was raised to 8.5 pJ. A further increase of the pulse energy to 12.5 pJ did not lead to an obvious increase of the luminescence intensity (see Video S1). This behavior is clearly revealed in the dependence of the luminescence intensity on the pulse energy shown in Figure 2b. The rapid increase of the luminescence intensity above a threshold is quite similar to that observed in amplified spontaneous emission.[32] Unfortunately, a line width narrowing is not observed in this case. Since the dramatic increase of the luminescence intensity agrees well with the exponential increase of carrier density at high temperatures, we think that the high temperature in the Si nanoparticle may trigger the intrinsic excitation which enhances the quantum efficiency (see Figure 1a,b). In Figure 2c, we compared the luminescence spectrum of the Si nanoparticle above the threshold with its scattering spectrum. It was found that the luminescence peak appears exactly at the MQ resonance. Based on the previous study on the modification of Mie resonances by injected carriers, the temperature of the Si nanoparticle was estimated to be ~1520 K (Figure S3, Supporting Information). We also examined the luminescence decays of the Si nanoparticle below and above the threshold, as shown Figure 2d. The lifetime above the threshold was found to be ~19 ps, which is shorter than that observed below the threshold (~50 ps). Although a decrease of τ_r is anticipated at high carrier densities, it is still

https://dx.doi.org/10.1021/acs.nanolett.0c04314
Nano Lett. XXXX, XXX, XXX−XXX

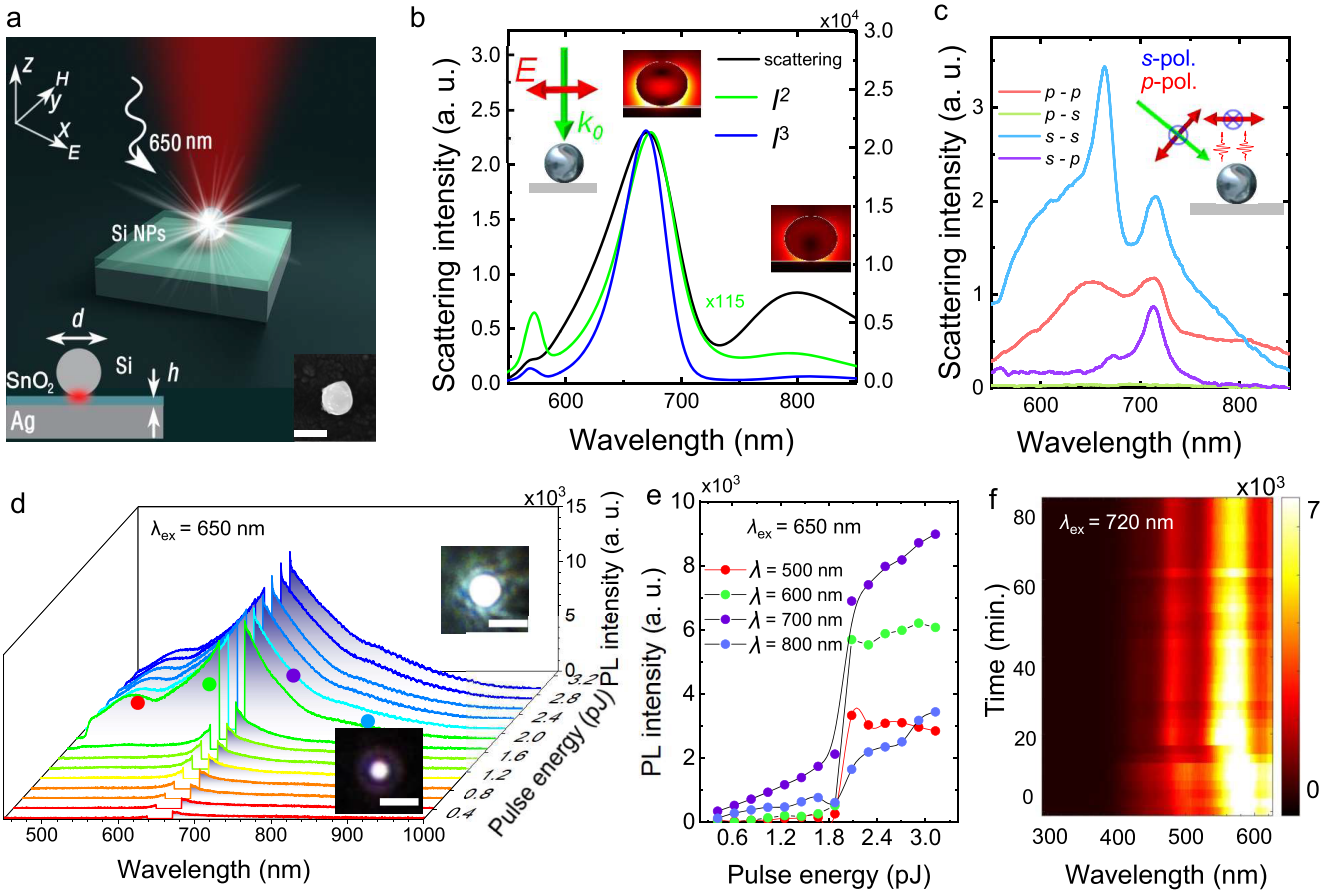

Figure 3. Luminescence burst observed for Si nanoparticles on a $SnO_2/Ag/SiO_2$ substrate. (a) Schematic showing the excitation of a Si nanoparticle placed on a $SnO_2/Ag/SiO_2$ substrate. The SEM image of a typical Si nanoparticle is shown in the inset. The length of the scale bar is 200 nm. The diameter of the Si nanoparticle is $d \sim 200$ nm. The thicknesses of the SnO_2 and Ag films are ~5.0 and ~50 nm, respectively. (b) Backward scattering spectrum calculated for a Si nanoparticle with $d = 200$ nm placed on a $SnO_2/Ag/SiO_2$ substrate. The spectra of $I^2 = [\int |E(\lambda)|^4 \, dV]/V$ and $I^3 = [\int |E(\lambda)|^6 \, dV]/V$ are presented to show the enhanced 2PA and 3PA. (c) Backward scattering spectra of a Si nanoparticle excited by using *p*- and *s*-polarized white light and filtered by using *p*- and *s*-polarized analyzers. (d) Evolution of the luminescence spectrum with increasing excitation pulse energy for the Si nanoparticle. The emissions of the Si nanoparticle recorded by using a charge coupled device below and above the threshold are shown in the insets. The length of the scale bar is 10 μm. The excitation wavelength was chosen to be $\lambda_{ex} = 650$ nm. (e) Dependence of the luminescence intensity on the excitation pulse energy measured for the Si nanoparticle at different wavelengths. (f) Evolution of the luminescence spectrum of a Si nanoparticle with $d \sim 200$ nm on the $SnO_2/Ag/SiO_2$ substrate, which was excited by femtosecond laser pulses at $\lambda_{ex} = 720$ nm, with increasing irradiation time.

much larger (about one order of magnitude) than τ_{nr} and the luminescence decay is still dominated by τ_{nr}. The reduction of τ_{nr} from 50 to 19 ps is caused mainly by the increase in the number of optical phonons at high temperatures.[31] We examined a few Si nanoparticles with their MD resonances at ~720 nm and observed similar behaviors. The thresholds for the luminescence burst ranged from 8.5 to 12.5 pJ. Above the threshold, the emission of Si nanoparticles became unstable and the damage of Si nanoparticles occurred easily due to overheating (Figure S4, Supporting Information).

In order to lower the threshold, we replaced the SiO_2 substrate with a $SnO_2/Ag/SiO_2$ substrate, as sketched in the inset of Figure 3a. Previously, a mode volume as small as $\sim \lambda^2/400$ was achieved by placing a CdSe nanowire on a $MgF_2/Ag/SiO_2$ substrate, which was exploited to realize the lasing of the CdSe nanowire.[33] In our case, the combination of a Si nanoparticle and a metal film is employed to create a tightly confined optical mode with a larger quality factor and a smaller mode volume,[34] leading to an enhancement in the Purcell factor (Figure S5, Supporting Information).

For optical characterization, we examined a Si nanoparticle with a diameter of $d \sim 200$ nm placed on a $SnO_2/Ag/SiO_2$ substrate. In Figure 3b, we show the backward scattering spectrum calculated for the Si nanoparticle. Owing to the existence of the Ag film, the total scattering is determined by the coherent interaction of ED/MD with their mirror images.[34−36] While the narrow scattering peak at ~670 nm with a quality factor of ~20 originates from the interference of the ED (p_x) and its mirror image (p_{xm}),[37] the broad one at ~800 nm arises from the MD (m_y) and its mirror image (m_{ym}).[36]

To examine the efficiencies of 2PA and 3PA,[38,39] we calculated the spectra of $I^2 = [\int |E(\lambda)|^4 \, dV]/V$ and $I^3 = [\int |E(\lambda)|^6 \, dV]/V$ for the Si nanoparticle, as shown in Figure 3b. It can be seen that the largest 2PA and 3PA are obtained at the mirror-image-induced MD with enhancement factors of ~190 and ~22000. As compared with the Si nanoparticle on the SiO_2 substrate (Figure S6, Supporting Information), the 2PA and 3PA have been enhanced by factors of ~4 and ~40, respectively. The enhanced electric field achieved at the

https://dx.doi.org/10.1021/acs.nanolett.0c04314
Nano Lett. XXXX, XXX, XXX−XXX

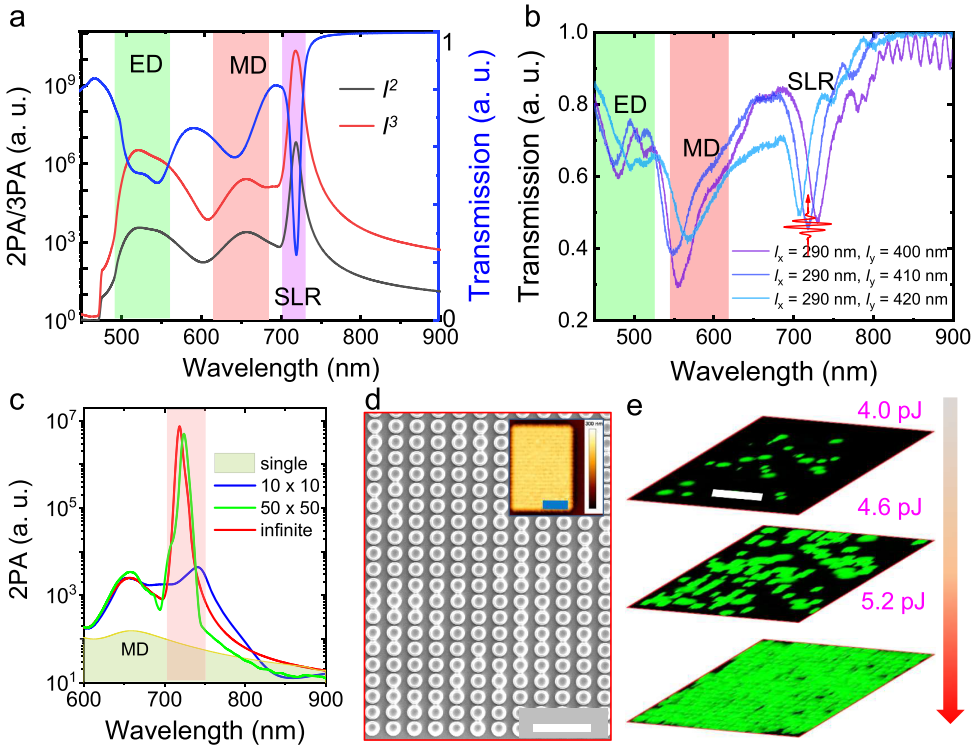

Figure 4. On chip Si-based white light source. (a) Transmission spectrum calculated for the rectangle lattice of Si nanopillars with l_y = 400 nm and l_x = 290 nm. The spectra of $I^2 = [\int |E(\lambda)|^4 \, dV]/V$ and $I^3 = [\int |E(\lambda)|^6 \, dV]/V$ are presented to show the enhanced 2PA and 3PA. (b) Transmission spectra measured for three rectangle lattices of Si nanopillars with l_y = 400, 410, and 420 nm and l_x = 290 nm. (c) Spectra of $I^2 = [\int |E(\lambda)|^4 \, dV]/V$ calculated for square lattices of Si nanopillars with different periods. The spectrum calculated for a single Si nanopillar is also provided. The spectrum for the infinitely large lattice (marked as 'infinite') was obtained by using a periodic boundary condition. (d) SEM image of the rectangle lattice of Si nanopillars with a diameter of ~250 nm (with 50 nm-thick SiO_2) and a height of ~220 nm. The AFM image after depositing the $SiNO_x$ layer is shown in the inset. The lengths of the scale bars are 1.0 and 6.0 μm in the SEM and AFM images, respectively. (e) Laser scanning confocal microscope images obtained by scanning the rectangle lattice of Si nanopillars with femtosecond laser pulses of different pulse energies and detecting the emitted hot electron luminescence. The length of the scale bar is 6.0 μm.

mirror-image-induced MD (~670 nm) is directly reflected in the electric field distribution shown in the inset of Figure 3b.

We measured the backward scattering spectra of a Si nanoparticle excited by *p*- and *s*- polarized white light and filtered by a *p*- or *s*-polarized analyzer, as shown in Figure 3c. The modified p_x mode (the mirror-image-induced MD) was revealed at ~670 nm in the scattering spectrum obtained by using the combination of the *s*-polarized white light and *s*-polarized analyzer. Similarly, the modified m_z mode was identified at ~720 nm by using the *s*-polarized white light and *p*-polarized analyzer. These observations agree well with those reported previously[36] (Figure S7, Supporting Information).

In our experiment, we chose to excite the mirror-image-induced MD by using an optical parametric oscillator and observed the luminescence burst, as shown in Figure 3d and e. It is remarkable that the threshold was dramatically reduced to be less than 2.0 pJ. Moreover, the stable emission above the threshold was realized, as shown in Figure 3f (see also Videos S2 and S3), due to the significantly reduced threshold and the good thermal conductivity of the Ag film. No rapid oxidation of the Si nanoparticle was observed because it was protected by the thin SiO_2 layer on the surface. The luminescence burst was reproducible for Si nanoparticles on the Ag film (Figure S8, Supporting Information). A small blue shift as well as a slight broadening was observed for the mirror-image-induced MD after the luminescence burst, in agreement with the small change in the morphology (Figure S9, Supporting Information). Owing to the large reflectivity of the Ag film, the collection efficiency of the luminescence is enhanced to ~52% (Figure S10, Supporting Information). We also measured the excitation spectra for the modified p_x and m_z modes and found a lower excitation efficiency for the latter one (Figure S11, Supporting Information).

In the previous study, the quantum efficiency for the luminescence of Si nanoparticles below the threshold was estimated to be ~1.00% if the 3PA was taken into account.[23] In this case, τ_{nr} was found to be ~50 ps and τ_r was deduced to be ~5.0 ns. It is expected that τ_r becomes inversely proportional to Δn when it exceeds 10^{20} cm^{-3} (see eq 2). For Si nanoparticles on a SiO_2 substrate, the luminescence burst was observed by increasing the carrier density to $\Delta n \sim 1.0 \times 10^{21}$ cm^{-3}. In this case, a reduction of τ_r from ~5.0 ns to ~500 ps is anticipated based on eq 2. Meanwhile, τ_{nr} is slightly reduced from ~50 ps to ~20 ps because of the high temperature (see Figure 2c). Consequently, the quantum efficiency above the threshold is estimated to be ~4.0%. By using the method proposed previously, we also estimated the quantum efficiencies for several Si nanoparticles placed on the Ag film (Figures S12–S15, Supporting Information) and found values ranging from 2.8% to 8.6% above the threshold, in good agreement with the above prediction based on the luminescence lifetime. Although a large increase in the quantum efficiency is not observed by placing Si nanoparticles on the Ag film, the improvement in the injection efficiency of

https://dx.doi.org/10.1021/acs.nanolett.0c04314
Nano Lett. XXXX, XXX, XXX−XXX

carriers leads to a dramatic reduction of the threshold, enabling the stable white light emission above the threshold. We calculated the blackbody radiation spectrum of a Si nanoparticle with d = 200 nm and estimated the thermal energy radiated from the Si nanoparticle in the wavelength range of 300−900 nm (Figure S16, Supporting Information). It was found that the thermal radiation from the Si nanoparticle is two orders of magnitude smaller than the optical radiation from a Si nanoparticle with the similar size. Moreover, it was found that the slope extracted from the dependence of the luminescence intensity of a Si nanoparticle on the pulse energy is nearly a constant (Figure S17, Supporting Information), which is distinct from that of a blackbody. Finally, the luminescence lifetime measured in the long-wavelength side was also as short as ∼20 ps (Figure S18, Supporting Information). All these behaviors indicate clearly that the emission from Si nanoparticles comes mainly from hot electron luminescence and that the thermal radiation is negligible.

As discussed above, the lifetime extracted from the luminescence decay is still governed by τ_{nr}. Although τ_r is expected to decrease at high carrier densities, it is still much longer than τ_{nr}. In addition, the luminescence lifetime above the threshold is close to the time resolution of the system. For these reasons, the emission intensities below and above the threshold do not match with the corresponding lifetimes. If we compared the quantum efficiencies below and above the threshold, we found that the increase in quantum efficiency agrees well with the enhancement in the emission intensity.

From the viewpoint of practical applications, it is necessary to fabricate all-Si-based light emitters on Si chips. Here, we show that the surface lattice resonance (SLR) originating from the periodic arrangement of Si nanoparticles can be employed to reduce the threshold and to sustain stable emission above the threshold. Basically, the constructive interference of the scattering light from regularly arranged scatters leads to the formation of SLRs in the reflection or transmission spectrum.[40−42] Here, we fabricated regularly arranged Si nanopillars on a Si-on-sapphire wafer by using the combination of electron beam lithography and plasma etching (see Methods for the details).

In our sample, the diameter and height of the Si nanopillars were designed to be 250 and 220 nm, respectively. The transmission spectrum calculated for a rectangle lattice of Si nanopillars with lattice constants of l_y = 400 nm and l_x = 290 nm is presented in Figure 4a (see Figure S19, Supporting Information). Apparently, a SLR appears at ∼720 nm where a significant enhancement of electric field is achieved, as manifested in the spectra of $I^2 = [\int |E(\lambda)|^4\, dV]/V$ and $I^3 = [\int |E(\lambda)|^6\, dV]/V$. It is remarkable that the enhancement factor of I^3 achieved at the SLR is increased by two orders of magnitude as compared with that obtained at the MD resonance of the Si nanopillar, implying a much higher efficiency for 3PA process.

In Figure 4b, we show the transmission spectra measured for three rectangle lattices of Si nanopillars with different lattice constants in the y direction l_y = 400, 410, and 420 nm (l_x = 290 nm). In all cases, one can find a transmission dip at ∼720 nm, corresponding to the SLR of the rectangle lattice. In Figure 4c, we show the evolution of the 2PA with increasing number of the period for the regular lattice with l_y = 410 nm and l_x = 290 nm. For the 50 × 50 rectangle lattice used in our experiment, the enhancement in the 2PA approaches the value for the infinitely large lattice. In Figure 4d, we present the scanning electron microscope (SEM) image for the rectangle array of Si nanopillars, which were capped by a $SiNO_x$ layer with a refractive index close to that of the sapphire substrate (Figure S20, Supporting Information). The atomic force microscope (AFM) image of the sample after capping the $SiNO_x$ layer is presented in the inset of Figure 4d. We employed a two-photon laser scanning confocal microscope to examine the luminescence of the Si nanopillars in the wavelength range of 550−650 nm. The images obtained by scanning the sample with different pulse energies are shown in Figure 4e where the burst phenomenon is also clearly identified. At low pulse energies, the burst phenomenon was observed only for Si nanopillars with lower thresholds. It spreads for nearly all the Si nanopillars at high pulse energies.

CONCLUDING REMARKS

In summary, we have proposed a new strategy for enhancing the quantum efficiency of hot electron luminescence of Si nanoparticles by exploiting the enhanced 2PA/3PA at various optical resonances. The strong dependences of the radiative and nonradiative recombination lifetimes on carrier density were exploited to modify the carrier dynamics and to improve the quantum efficiency. The new findings and insights of this work include (1) the observation of hot electron luminescence burst in Si nanoparticles on a SiO_2 substrate by resonantly exciting their MD resonances at ∼720 nm; (2) the reduction of the threshold for luminescence burst and the realizing of stable white light emission by resonantly exciting the mirror-image-induced MDs of Si nanoparticles placed on a thin Ag film; (3) the observation of luminescence burst and the realizing of efficient white light emission by exploiting the surface lattice resonance of a regular array of Si nanopillars fabricated by using the current fabrication technology of Si chips; (4) the observation that the emission from Si nanoparticles at high temperatures is still dominated by hot electron luminescence rather than thermal radiation; and (5) the observation that the quantum efficiency is further enhanced by a factor of ∼5.0 above the threshold for the luminescence burst. Our findings are helpful for understanding the carrier dynamics at extremely high carrier densities and are useful for designing highly efficient Si-based nanoscale light sources for integrated optical circuits.

METHODS

Fabrication of Si Nanoparticles and Regular Arrays of Si Nanopillars. In experiments, an 800 nm femtosecond laser light delivered by a femtosecond amplifier (Legend Elite, Coherent) with a pulse duration of 90 fs and a repetition rate of 1 kHz was focused on the surface of a crystalline-Si wafer, which was immersed in deionized water, by using a lens with a focal length of 150 mm. Then, the aqueous solution containing Si nanoparticles was centrifuged with a speed of 12000 rpm to separate Si nanoparticles with diameters of 150−250 nm from small Si nanoparticles. Finally, Si nanoparticles with appropriate diameters were dispersed on a SiO_2 substrate or a SnO_2/Ag/SiO_2 substrate for optical characterization.

We fabricated regularly arranged Si nanopillars on a Si-on-sapphire wafer composed of a 220 nm thick c-Si and a 500 μm thick sapphire by using the combination of electron beam lithography and plasma etching. The nanopillar array was first defined in high-resolution negative resist (hydrogen silsesquioxane) by using electron beam lithography (Vistec EBPG-

https://dx.doi.org/10.1021/acs.nanolett.0c04314
Nano Lett. XXXX, XXX, XXX−XXX

5000plusES, Raith) at 100 keV. The spin speed and baking condition of HSQ were 4000 rpm and 90° for 4 min, respectively. Then, the pattern was developed in a solution of tetramethylammonium hydroxide and dry etched by using inductively coupled plasma etching (Oxford Instruments). The method for fabricating Si nanopillars was the same as those described in previous works.[23,43] After the remaining resist was removed by hydrofluoric acid, dry thermal oxidation was employed to form a thin SiO_2 layer (~50 nm) in order to remove the surface defects induced in plasma etching. Dry thermal oxidation was carried out in a tube furnace at 1000 °C with an oxygen flow of 0.90 slm (standard liters per minute) for 100 min. Argon (1.0 slm) was used to protect the samples from oxidation during the heating and cooling of the tube furnace. Finally, a $SiNO_x$ layer with the same refractive index of the sapphire substrate was capped on the Si nanopillars.

Optical Characterization of Si Nanoparticles. The backward scattering spectra of Si nanoparticles were measured by using a dark-field microscope (Observer A1, Zeiss) with an external white light source for illumination. The incident light can be either *s*- or *p*-polarized by using a polarizer. The femtosecond laser light was introduced into an inverted microscope (Observer A1, Zeiss) and focused on Si nanoparticles by using a 100× objective. The hot electron luminescence emitted by Si nanoparticles was collected by using the same objective and directed to a spectrometer (SR500, Andor) for analysis. We used a two-photon laser scanning confocal microscope (A1MP, Nikon) to excite and detect the hot electron luminescence emitted from the regular arrays of Si nanopillars.

Measurement of the Luminescence Lifetime. We measured the luminescence decay time of Si nanoparticles by using a fluorescence lifetime spectrometer (LifeSpec-1400, Edinburgh Instruments) equipped with a microchannel plate photomultiplier (Hamamatsu). The luminescence decays were analyzed by using the F900 software package (ver. 7.1.3), and the decay times were extracted based on a deconvolution fitting analysis in which the instrumental response function was taken into account.

Numerical Modeling. The scattering spectra of Si nanoparticles and the transmission spectra of the regular arrays of Si nanopillars were numerically simulated by using the finite-difference time-domain (FDTD) technique based on the complex refractive indices of crystalline silicon and silver.[44] For the scattering spectra, we employed a total-field/scattered-field source to evaluate the scattering efficiency of Si nanoparticles. A uniform mesh size with the smallest one of 1 nm was used to obtain converged simulation results, and a perfectly matched layer boundary condition was employed to terminate the finite simulation region. For the transmission spectra, a plane wave was used to excite the regular arrays of Si nanopillars, and a periodic boundary condition was employed in the numerical simulations.

■ ASSOCIATED CONTENT

Supporting Information

The Supporting Information is available free of charge at https://pubs.acs.org/doi/10.1021/acs.nanolett.0c04314.

Detailed information about sample preparation, morphology characterization, optical measurements, including scattering, luminescence, quantum efficiency, etc., and numerical simulation (PDF)

Video S1 (MP4)

Video S2 (MP4)

ZIP file containing Video S3 (ZIP)

■ AUTHOR INFORMATION

Corresponding Authors

Juntao Li − *State Key Laboratory of Optoelectronic Materials and Technologies, School of Physics, Sun Yat-sen University, Guangzhou 510275, People's Republic of China*; Email: lijt3@mail.sysu.edu.cn

Sheng Lan − *Guangdong Provincial Key Laboratory of Nanophotonic Functional Materials and Devices, School of Information and Optoelectronic Science and Engineering, South China Normal University, Guangzhou 510006, People's Republic of China*; orcid.org/0000-0002-7277-0042; Email: slan@scnu.edu.cn

Authors

Jin Xiang − *Guangdong Provincial Key Laboratory of Nanophotonic Functional Materials and Devices, School of Information and Optoelectronic Science and Engineering, South China Normal University, Guangzhou 510006, People's Republic of China*; orcid.org/0000-0003-0896-7526

Mincheng Panmai − *Guangdong Provincial Key Laboratory of Nanophotonic Functional Materials and Devices, School of Information and Optoelectronic Science and Engineering, South China Normal University, Guangzhou 510006, People's Republic of China*

Shuwen Bai − *Guangdong Provincial Key Laboratory of Nanophotonic Functional Materials and Devices, School of Information and Optoelectronic Science and Engineering, South China Normal University, Guangzhou 510006, People's Republic of China*

Yuhao Ren − *State Key Laboratory of Optoelectronic Materials and Technologies, School of Physics, Sun Yat-sen University, Guangzhou 510275, People's Republic of China*

Guang-Can Li − *Guangdong Provincial Key Laboratory of Nanophotonic Functional Materials and Devices, School of Information and Optoelectronic Science and Engineering, South China Normal University, Guangzhou 510006, People's Republic of China*; orcid.org/0000-0002-9903-8900

Shulei Li − *Guangdong Provincial Key Laboratory of Nanophotonic Functional Materials and Devices, School of Information and Optoelectronic Science and Engineering, South China Normal University, Guangzhou 510006, People's Republic of China*; orcid.org/0000-0001-9346-3773

Jin Liu − *State Key Laboratory of Optoelectronic Materials and Technologies, School of Physics, Sun Yat-sen University, Guangzhou 510275, People's Republic of China*

Miaoxuan Zeng − *State Key Laboratory of Optoelectronic Materials and Technologies, Guangdong Province Key Laboratory of Display Material and Technology, School of Electronics and Information Technology, Sun Yat-sen University, Guangzhou 510275, People's Republic of China*

Juncong She − *State Key Laboratory of Optoelectronic Materials and Technologies, Guangdong Province Key Laboratory of Display Material and Technology, School of Electronics and Information Technology, Sun Yat-sen University, Guangzhou 510275, People's Republic of China*; orcid.org/0000-0002-5483-3636

https://dx.doi.org/10.1021/acs.nanolett.0c04314
Nano Lett. XXXX, XXX, XXX−XXX

Yi Xu − *Department of Electronic Engineering, College of Information Science and Technology, Jinan University, Guangzhou 510630, People's Republic of China*

Complete contact information is available at: https://pubs.acs.org/10.1021/acs.nanolett.0c04314

Author Contributions

J.X. and M.P. contributed equally to this work. S. Lan, J. Li, and J.X. conceived the idea. J.X., Y.R., and M.Z. fabricated the Si nanoparticles and regular arrays of Si nanopillars and performed morphology characterization. J.X., M.P., S.B., G.L., and S.L. carried out the optical measurements and numerical simulations. S. Lan, J. Li, and J.X. analyzed the data and wrote the manuscript. S. Lan, J. Li, J. Liu, Y.X., and J.S. supervised the project. All of the authors read and commented on the manuscript.

Notes

The authors declare no competing financial interest.

■ ACKNOWLEDGMENTS

The authors acknowledge the financial support from the National Key Research Program of China (1016YFA0201002), the National Natural Science Foundation of China (11674110, 11874020, 11974436 and 61874144), the Natural Science Foundation of Guangdong Province, China (2016A030308010, 2018B030311045), and the Guangdong Basic and Applied Basic Research Foundation (2020B1515020019).

■ REFERENCES

(1) Priolo, F.; Gregorkiewicz, T.; Galli, M.; Krauss, T. F. Silicon nanostructures for photonics and photovoltaics. *Nat. Nanotechnol.* **2014**, *9*, 19−32.
(2) Xu, Q. F.; Schmidt, B.; Pradhan, S.; Lipson, M. Micrometre-scale silicon electro-optic modulator. *Nature* **2005**, *435*, 325−327.
(3) Almeida, V. R.; Barrios, C. A.; Panepucci, R. R.; Lipson, M. All-optical control of light on a silicon chip. *Nature* **2004**, *431*, 1081−1084.
(4) Almeida, V. R.; Xu, Q. F.; Barrios, C. A.; Lipson, M. Guiding and confining light in void nanostructure. *Opt. Lett.* **2004**, *29*, 1209−1211.
(5) Fama, S.; Colace, L.; Masini, G.; Assanto, G.; Luan, H. C. High performance germanium-on- silicon detectors for optical communications. *Appl. Phys. Lett.* **2002**, *81*, 586−588.
(6) de Boer, W. D. A. M.; et al. Red spectral shift and enhanced quantum efficiency in phonon-free photoluminescence from silicon nanocrystals. *Nat. Nanotechnol.* **2010**, *5*, 878−884.
(7) Timmerman, D.; Valenta, J.; Dohnalova, K.; de Boer, W.; Gregorkiewicz, T. Step-like enhancement of luminescence quantum yield of silicon nanocrystals. *Nat. Nanotechnol.* **2011**, *6*, 710−713.
(8) Dohnalova, K.; et al. Surface brightens up Si quantum dots: direct bandgap-like size-tunable emission. *Light: Sci. Appl.* **2013**, *2*, No. e47.
(9) Wang, L.; et al. Ultrafast optical spectroscopy of surface-modified silicon quantum dots: unraveling the underlying mechanism of the ultrabright and color-tunable photoluminescence. *Light: Sci. Appl.* **2015**, *4*, No. e245.
(10) Ginn, J. C.; et al. Realizing Optical Magnetism from Dielectric Metamaterials. *Phys. Rev. Lett.* **2012**, *108*, 097402.
(11) Fu, Y. H.; Kuznetsov, A. I.; Miroshnichenko, A. E.; Yu, Y. F.; Luk'yanchuk, B. Directional visible light scattering by silicon nanoparticles. *Nat. Commun.* **2013**, *4*, 1527.
(12) Kuznetsov, A. I.; Miroshnichenko, A. E.; Brongersma, M. L.; Kivshar, Y. S.; Luk'yanchuk, B. Optically resonant dielectric nanostructures. *Science* **2016**, *354*, aag2472.
(13) Staude, I.; Schilling, J. Metamaterial-inspired silicon nanophotonics. *Nat. Photonics* **2017**, *11*, 274−284.
(14) Xiang, J.; et al. Manipulating the Orientations of the Electric and Magnetic Dipoles Induced in Silicon Nanoparticles for Multicolor Display. *Laser & Photonics Rev.* **2018**, *12*, 1800032.
(15) Koshelev, K.; Favraud, G.; Bogdanov, A.; Kivshar, Y.; Fratalocchi, A. Nonradiating photonics with resonant dielectric nanostructures. *Nanophotonics* **2019**, *8*, 725−745.
(16) Liu, W.; Kivshar, Y. S. Generalized Kerker effects in nanophotonics and meta-optics. *Opt. Express* **2018**, *26*, 13085−13105.
(17) Cihan, A. F.; Curto, A. G.; Raza, S.; Kik, P. G.; Brongersma, M. L. Silicon Mie resonators for highly directional light emission from monolayer MoS_2. *Nat. Photonics* **2018**, *12*, 284−290.
(18) Panmai, M. C.; et al. All silicon-based nano-antennas for wavelength and polarization demultiplexing. *Opt. Express* **2018**, *26*, 12344−12362.
(19) Shcherbakov, M. R.; et al. Enhanced third-harmonic generation in silicon nanoparticles driven by magnetic response. *Nano Lett.* **2014**, *14*, 6488−6492.
(20) Liu, S.; et al. Resonantly Enhanced Second-Harmonic Generation Using III-V Semiconductor All-Dielectric Metasurfaces. *Nano Lett.* **2016**, *16*, 5426−5432.
(21) Shorokhov, A. S.; et al. Multifold Enhancement of Third-Harmonic Generation in Dielectric Nanoparticles Driven by Magnetic Fano Resonances. *Nano Lett.* **2016**, *16*, 4857−4861.
(22) Makarov, S. V.; et al. Efficient Second-Harmonic Generation in Nanocrystalline Silicon Nanoparticles. *Nano Lett.* **2017**, *17*, 3047−3053.
(23) Zhang, C.; et al. Lighting up silicon nanoparticles with Mie resonances. *Nat. Commun.* **2018**, *9* (1), 2964.
(24) Xiang, J.; et al. Modifying Mie Resonances and Carrier Dynamics of Silicon Nanoparticles by Dense Electron-Hole Plasmas. *Phys. Rev. Appl.* **2020**, *13*, 014003.
(25) Ha, S. T.; et al. Directional lasing in resonant semiconductor nanoantenna arrays. *Nat. Nanotechnol.* **2018**, *13*, 1042.
(26) Mylnikov, V.; et al. Lasing action in single subwavelength particles supporting supercavity modes. *ACS Nano* **2020**, *14*, 7338−7346.
(27) Zhang, T. Y.; et al. Anapole mediated giant photothermal nonlinearity in nanostructured silicon. *Nat. Commun.* **2020**, *11*, 3027.
(28) Haug, T.; Klemm, P.; Bange, S.; Lupton, J. M. Hot-electron intraband luminescence from single hot Spots in noble-metal nanoparticle films. *Phys. Rev. Lett.* **2015**, *115*, 067403.
(29) Xiang, J.; et al. Hot-electron intraband luminescence from GaAs nanospheres mediated by magnetic dipole resonances. *Nano Lett.* **2017**, *17*, 4853−4859.
(30) Cho, C.-H.; Aspetti, C. O.; Park, J.; Agarwal, R. Silicon coupled with plasmon nanocavities generates bright visible hot luminescence. *Nat. Photonics* **2013**, *7*, 285−289.
(31) Li, S. S. *Semiconductor Physical Electronics*, 2nd ed.; Springer: New York, 2006.
(32) Xing, G. C.; et al. Ultralow-Threshold Two-Photon Pumped Amplified Spontaneous Emission and Lasing from Seeded CdSe/CdS Nanorod Heterostructures. *ACS Nano* **2012**, *6*, 10835−10844.
(33) Oulton, R. F.; Sorger, V. J.; Zentgraf, T.; Ma, R. M.; Gladden, C.; Dai, L.; Bartal, G.; Zhang, X. Plasmon lasers at deep subwavelength scale. *Nature* **2009**, *461*, 629−632.
(34) Xifre-Perez, E.; et al. Mirror-image-induced magnetic modes. *ACS Nano* **2013**, *7*, 664−668.
(35) Miroshnichenko, A. E.; Evlyukhin, A. B.; Kivshar, Y. S.; Chichkov, B. N. Substrate-Induced Resonant Magnetoelectric Effects for Dielectric Nanoparticles. *ACS Photonics* **2015**, *2*, 1423−1428.
(36) Sinev, I.; et al. Polarization control over electric and magnetic dipole resonances of dielectric nanoparticles on metallic films. *Laser & Photonics Rev.* **2016**, *10*, 799−806.
(37) Li, H.; et al. Exploiting the interaction between a semiconductor nanosphere and a thin metal film for nanoscale plasmonic devices. *Nanoscale* **2016**, *8*, 18963−18971.

(38) Ghenuche, P.; Cherukulappurath, S.; Taminiau, T. H.; van Hulst, N. F.; Quidant, R. Spectroscopic mode mapping of resonant plasmon nanoantennas. *Phys. Rev. Lett.* **2008**, *101*, 116805.
(39) Viarbitskaya, S.; et al. Tailoring and imaging the plasmonic local density of states in crystalline nanoprisms. *Nat. Mater.* **2013**, *12*, 426−432.
(40) Kravets, V. G.; Schedin, F.; Grigorenko, A. N. Extremely narrow plasmon resonances based on diffraction coupling of localized plasmons in arrays of metallic nanoparticles. *Phys. Rev. Lett.* **2008**, *101*, 087403.
(41) Babicheva, V. E.; Evlyukhin, A. B. Resonant Lattice Kerker Effect in Metasurfaces With Electric and Magnetic Optical Responses. *Laser & Photonics Rev.* **2017**, *11*, 1700132.
(42) Kravets, V. G.; Kabashin, A. V.; Barnes, W. L.; Grigorenko, A. N. Plasmonic Surface Lattice Resonances: A Review of Properties and Applications. *Chem. Rev.* **2018**, *118*, 5912−5951.
(43) Xiang, J.; Li, J.; Zhou, Z.; Jiang, S.; Chen, J.; Dai, Q.; Tie, S.; Lan, S.; Wang, X. 2018. Manipulating the orientations of the electric and magnetic dipoles induced in silicon nanoparticles for multicolor display. *Laser & Photonics Reviews* **2018**, *12*, 1800032.
(44) Palik, E. D. *Handbook of Optical Constants of Solids*; Academic Press: New York, 1998.

https://dx.doi.org/10.1021/acs.nanolett.0c04314
Nano Lett. XXXX, XXX, XXX−XXX